

Field-free superconducting diode effect in layered superconductor FeSe

Utane Nagata¹, Motomi Aoki^{1,2}, Akito Daido³, Shigeru Kasahara⁴, Yuichi Kasahara³, Ryo Ohshima^{1,2}, Yuichiro Ando^{1,2}, Youichi Yanase^{2,3}, Yuji Matsuda³ and Masashi Shiraishi^{1,2†}

¹Department of Electronic Science and Engineering, Kyoto University, Kyoto, Kyoto 615-8510, Japan

²Center for Spintronics Research Network, Institute for Chemical Research, Kyoto University, Uji, Kyoto 611-0011, Japan

³Department of Physics, Graduate School of Science, Kyoto University, Kyoto 606-8502, Japan

⁴ Research Institute for Interdisciplinary Science, Okayama University, Okayama, 700-8530, Japan

Corresponding authors

Masashi Shiraishi

E-mail: shiraishi.masashi.4w@kyoto-u.ac.jp

The superconducting diode effect (SDE), where zero-resistance states appear nonreciprocally during current injection, is receiving tremendous interest in both fundamental and applied physics because the SDE is a novel manifestation of symmetry breaking and enables the creation of a novel diode without energy loss. In particular, magnetic-field-free SDEs have been extensively investigated because of their potential to serve as building blocks for superconducting circuit technology. In this letter, we report the field-free SDE in a layered superconductor, FeSe. Its underlying physics is clarified by systematic controlled experiments to be an interplay of a large thermoelectric response and geometrical asymmetry in FeSe. Our findings can pave a new avenue for the construction of novel material and device platforms utilizing SDEs.

Symmetry breaking provides a wide variety of abundant physical nature. The breaking of the spatial inversion symmetry enables the creation of the diode effect, which plays a dominant role in the information rectification in electronics, and the so-called Rashba effect, which has been and is still intensively investigated in view of spintronics. Time reversal symmetry breaking is accompanied by magnetic ordering, resulting in the anomalous Hall effect and related intriguing spintronics traits. The combination of the spatial inversion and time reversal symmetries can render condensed matter physics more plentiful. In fact, the increase in topological quantum materials stems from the spatial inversion symmetry breaking with preservation of the time reversal symmetry. The other significant manifestation of the symmetry combination, where both the spatial inversion and time reversal symmetries are broken, is nonreciprocal transport [1–3]. Nonreciprocal transport is a family of rectification effects in which the amplitudes of the electric current flowing in the opposite directions are not the same; specifically, a nonlinear response beyond Onsager's reciprocity occurs. Since the first experimental demonstration of nonreciprocal charge transport in a Si metal-on-semiconductor field effect transistor [3], this novel function in charge transport has attracted the attention of many researchers [4–8].

The superconducting diode effect (SDE) is categorized as a family of nonreciprocal charge transport. The amplitudes of the supercurrent (not the charge current) flowing in the opposite directions are not the same, resulting in a shift in the critical current due to the breaking of the superconductivity when the supercurrent exceeds the critical current in one direction [9]. In the SDE, the spatial inversion and time reversal symmetries are simultaneously broken by the so-called tricolor stacking of Nb/V/Ta and an external in-plane magnetic field, respectively; both of these are indispensable for nonreciprocal transport. In theory, spatial inversion breaking gives rise to the Rashba-type helical spin structure, and the time reversal symmetry breaking allows the Cooper pairs in the system to acquire finite momentum; this process is the inherent mechanism of the SDE [10] and signifies the importance of the symmetry breaking combination. In subsequent studies, many material platforms have been reported for the appearance of the SDE [11–13], and a variety of other mechanisms, such as asymmetric tunnelling at the Josephson junction [14–17], magnet chiral anisotropy (MCA) at the surface state of topological superconductors [18], and Josephson vortices in multilayered superconducting nanowires [19], have been proposed. Furthermore, whereas numerous research has been performed to explain the detailed

underlying physics from theoretical perspectives [20–24], it was recently determined that the phenomenological Ginzburg–Landau theory cannot explain the full nature of the SDE [25]. Importantly, although the SDE platforms reported thus far commonly possess structural asymmetry (interfaces, junctions, and crystal structures with a broken inversion symmetry), time reversal symmetry breaking is not always required. Indeed, the field-free Josephson diode effect (JDE) [14], where an external magnetic field to break the time reversal symmetry is not applied, takes place in some material systems with inversion symmetry breaking, and its underlying physics is still elusive. Furthermore, a recent systematic investigation of the SDE [26] revealed that the occurrence of the SDE is irrelevant to the finite-momentum pairing, which requests revisiting the conventional SDE results. Thus, a quest of further precise understandings of the physics behind the SDE that is currently somewhat intricately intertwined is strongly awaited and significant.

In this letter, we report the observation of a field-free SDE in a layered superconductor, FeSe, with a symmetric crystal structure. Although the spatial inversion symmetry in the crystal and time reversal symmetry are conserved in FeSe, the salient SDE is surprisingly observed in both the dc and the second harmonic voltage measurements, which are compelling evidence for the SDE. We successfully corroborated that the field-free SDE in this work was attributed to the interplay of a sample-geometry-induced thermal gradient and thermoelectric effect in FeSe, which is clearly supported by the control experiments using NbN with a similar geometry but different thermoelectric traits. Our study elucidates a novel physical aspect of the SDE, the thermoelectric contribution, and enables the expansion of material platforms for the SDE. Furthermore, our study enables delving further into the field-free SDEs by requesting to revisit the sample geometries and thermoelectric characteristics of the materials introduced thus far.

Figure 1(a) shows a schematic of the SDE appearing in an FeSe flake. FeSe is a family of iron-chalcogenide superconductors that possess layered and spatially symmetric crystal structures (see Fig. 1(b)) [27]. FeSe was exfoliated and transferred onto a thermally oxidized Si substrate. The thickness of the FeSe flake was approximately 114 nm. Since the superconducting transition is suppressed when FeSe is thinner than 20–30 nm, which is almost consistent with the result shown in ref. [28], we set the thickness of the FeSe to be greater than 30 nm. Rectangular Au (100 nm) electrodes were fabricated on the FeSe flakes by using electron-beam (EB)

lithography and EB deposition following Ar^+ ion milling in a load-lock chamber enabling Ohmic contact with the FeSe. Nonmagnetic Ti (3 nm)/Au (150 nm) pads connected to the Au electrodes on the FeSe were fabricated using EB lithography and EB deposition. Notably, neither the Josephson junction nor the stacking structures that break inversion symmetry existed in the device, and ferromagnetic electrodes to break the time reversal symmetry were not exploited. Figure 1(c) shows the measurement setup for the SDE, where the four-terminal voltage was measured between electrodes 2 and 3, and measurements were carried out using a physical property measurement system (PPMS; Quantum Design). The superconducting trait of FeSe was corroborated by the temperature dependence of the four-terminal resistance, and the midpoint superconducting transition temperature T_c^{mid} was determined to be 13 K (see Fig. 1(d)).

Distinct shifts in the critical current $\Delta I_c = I_{c+} - I_{c-}$, where $I_{c+(-)}$ is the critical current under positive (negative) current application, were detected in FeSe below 10 K without an external magnetic field as manifestation of the field-free SDE in FeSe. Figure 2(a) shows the I - V characteristics as a function of temperature of the FeSe device. ΔI_c increased as the temperature decreased and reached to 92 μA at 4 K. The amplitude of ΔI_c greatly exceeded the current sweeping step (4 μA). To confirm a response to an external magnetic field, B_{ext} , applied perpendicular to the current flow direction, ΔI_c was measured with respect to the in-plane external magnetic field (see Fig. 2(b)). ΔI_c is immune to B_{ext} and does not exhibit the odd function behavior with respect to B_{ext} unlike the conventional SDE, and thus, time reversal symmetry breaking is not necessary for the SDE in FeSe.

The measurement using an AC electric current, I_{AC} , with a frequency of 17 Hz provides compelling evidence for the observation of the field-free SDE in FeSe. Figure 3(a) shows the first and second harmonic resistances (R_ω and $R_{2\omega}$) as a function of the AC current. A salient peak in $R_{2\omega}$ was observed at an I_{AC} of ~ 0.89 mA, where a sharp increase in R_ω due to the superconducting to normal state transition occurred. Given that the $R_{2\omega}$ is attributed to the rectification effect, the amplification of $R_{2\omega}$ around the critical current buttresses the successful observation of the difference in I_{c+} and I_{c-} [9]. In addition, the magnitude of the peak of the second harmonic voltage gradually and monotonically decreased as the temperature increased up to T_c and approached zero at 15 K, where the FeSe transitioned to the normal conducting state as shown in Fig. 3(b). This finding is

consistent with the monotonic decrease in ΔI_c with increasing temperature, as shown in Fig. 2(a). To obtain further supporting evidence of the field-free SDE in FeSe, DC electric currents of +0.77 mA and -0.77 mA were applied alternately for 50 cycles, where the current amplitude was set between I_{c+} and I_{c-} at 6 K (see the upper panel of Fig. 3(c)). The FeSe exhibited a zero-resistance superconducting state when +0.77 mA was applied, whereas the resistance was nonzero under the application of -0.77 mA. In addition, the SDE was also robust for 50 cycles. These supporting results underscore the validity of our assertion of the successful detection of the field-free SDE in FeSe.

Since FeSe has a symmetric crystal structure and ΔI_c does not show discernible B_{ext} dependence, the conventional understanding of the SDE, where the breaking of the spatial inversion and time reversal symmetries is simultaneously requested, does not hold in the field-free SDE in FeSe. In particular, the absence of an external magnetic field in the SDE in FeSe is reminiscent of the similar SDE, the field-free Josephson diode effect [14], because the spatial inversion symmetry is broken along the perpendicular to the FeSe; this is analogous to breaking along the stacking plane of $\text{NbSe}_2/\text{Nb}_3\text{Br}_8/\text{NbSe}_2$. Meanwhile, the underlying physics of the field-free Josephson diode effect are still elusive, whereas nonreciprocal tunneling with out-of-plane polarization may be a relevant origin. Since a single FeSe layer allows manifestation of the field-free SDE, construction of another model to understand the physics of the field-free SDE in FeSe is required. Indeed, the ΔI_c is unchanged and exhibits even behavior to a weak magnetic field within 1 mT, which can be compelling evidence that the field-free SDE in FeSe is not attributable to the Meissner screening enabling the ubiquitous SDE [26] because the ubiquitous SDE is sensitive to the external magnetic field (see also Supplemental Material F [29] for more detail of the control experiments). The fact that the ΔI_c is immune to the external magnetic field of up to 9 T allows negating that excess Fe atoms in FeSe play the role of time reversal symmetry breaking as well (see also Supplemental Material H [29] about the immunity of the ΔI_c to the magnetic field). Given that the SDE manifests itself at around the critical electric current, where the superconducting to normal (and *vice versa*) transition takes place and that FeSe exhibits substantial heat response as the large Seebeck coefficient in the normal state, the Joule heating of FeSe in the normal state above the critical current can attribute to the findings. The geometry of the FeSe flake is not isotropic but rather triangular-like (see Fig. 1(c)) and the electric current

injected from the Au electrode can produce Joule heating due to contact resistance concomitant with the electrode. The heat generated at the contact at the wider side of the FeSe flake dissipates along the in-plane direction more significantly than that at the narrower side since the thermal dissipation is correlated with the thermal conductance, i.e., the width of the FeSe flake. Consequently, the temperature at the narrower side of the flake becomes higher than that at the wider side as shown in Fig. 4(a), and an in-plane temperature gradient ∇T is generated between electrodes 3 and 6 in the FeSe device (see Supplementary Materials B and C [29]). Thermal transport occurs in both normal conductors and superconductors via quasiparticles [30], and the thermal response of FeSe is substantially large (the Seebeck coefficient of FeSe in the normal state at low temperature is approximately $-10 \mu\text{V/K}$ [31]); thus, the in-plane thermal gradient in the FeSe can produce an additional charge current density, i_{th} . This results in the addition (cancellation) of the net current density flowing in the FeSe flake when i_{th} is parallel (antiparallel) to I (see also Fig. 4(a)) at a certain temperature and/or in the electric current range, where the superconductivity is close to being broken. When the net current density exceeds the critical current density, i_c , the superconductivity of the FeSe thermally breaks, and the FeSe transitions to the normal state, which can qualitatively explain the experimental results. Furthermore, we verified that the field-free SDE vanishes in FeSe when the shape of the FeSe flake is not asymmetric, which strongly supports our assertion (see Figs. 4(b) and 4(c)). This result also confirms that time reversal symmetry breaking in twin boundaries of FeSe [32] is NOT the origin of the field-free SDE. Notably, our control experiments using $\text{FeTe}_{0.6}\text{Se}_{0.4}$ (FTS), which possesses the large Seebeck coefficient in the normal state at low temperature ($-10 \mu\text{V/K}$ [33]) and is the other family of iron-chalcogenide superconductors, also exhibited a similar field-free SDE (see Supplemental Material D [29]). To obtain further supporting evidence that the field-free SDE in FeSe is attributed to the thermal gradient-induced phenomenon, we prepared a NbN film (103 nm thick), of which shape is quite similar to the shape of the FeSe flake (see Fig. 5(a) and [29] for the details of the fabrication). Since the thermoelectric response of NbN is much weaker than that of FeSe (the Seebeck coefficient of NbN in the normal state at low temperature is approximately $0.1 \mu\text{V/K}$ [34]), we deduce that NbN cannot exhibit a field-free SDE even when shape anisotropy exists. In fact, ΔI_c of the NbN device is indiscernible, indicating that the field-free SDE is absent in the NbN film with a similar asymmetric structure as the FeSe and FTS investigated in this

study, which underscores the validity of our assertion. We note that the device with the NbN channel that is the complete mimic of the FeSe channel in size, structure and geometry exhibited suppression of the SDE (see Supplemental Material I [29]), which is strong supporting evidence that the field-free SDE of FeSe is not attributed to Meissner screening and/or asymmetric vortex barriers [26,35,36] that are sensitive to asymmetric or serrated edge structures of superconductors. Furthermore, the FeSe devices with a sharp and a serrated edges exhibit almost the same field-free SDE, which is additional evidence that the thermoelectric response in FeSe, not the edge structure of it, plays a pivotal role in manifestation of SDE (see Supplemental Material J [29]). In consequence, all field-free SDE results obtained using materials with various thermal responses unequivocally show that the origin of the field-free SDE in FeSe is the thermal gradient due to asymmetry in the shape of the FeSe flake.

In summary, we found a field-free SDE in a layered superconductor FeSe film, the origin of which was determined to the in-plane temperature gradient due to Joule heating generated at the contact resistance and asymmetric shape of the FeSe flake. Despite the simple device structure composed of only FeSe flake and nonmagnetic electrodes, half-wave rectification between the superconducting and normal states was successfully demonstrated. Since the SDE induced by heat dissipation was generated simply by shaping a material with a large thermoelectric coefficient into an asymmetric shape, our findings can open a novel pathway for achieving energy-efficient logic devices utilizing the SDE. Furthermore, our finding requests revisiting previous experimental setups in the field-free SDE, where asymmetric structures in superconducting channels and/or materials exhibiting large thermal response are exploited, in view of thermal dissipation.

Acknowledgements

This work is partly supported by JSPS Grant-in-Aid for Challenging Research (Pioneering) (23K17353, 21K18145 and 19H05522), Grant-in-Aid for Scientific Research (B) (22H01181), Grant-in-Aid for Scientific Research (S) (22H04933), Grant-in-Aid for Early-Career Scientists (21K13880), and Grant-in-Aid for Transformative Research Areas (24H01662). U.N., M.A., R.O, Y.A. and M.S. would like to thank Dr. E. Tamura for his fruitful discussion.

Data availability

The data that support the findings of this study are available from the corresponding author upon reasonable request.

References

- [1] G. L. J. A. Rikken and E. Raupach, *Observation of Magneto-Chiral Dichroism*, *Nature* **390**, 493 (1997).
- [2] G. L. J. A. Rikken, J. Fölling, and P. Wyder, *Electrical Magnetochiral Anisotropy*, *Phys. Rev. Lett.* **87**, 236602 (2001).
- [3] G. L. J. A. Rikken and P. Wyder, *Magnetoelectric Anisotropy in Diffusive Transport*, *Phys. Rev. Lett.* **94**, 016601 (2005).
- [4] K. Yasuda, A. Tsukazaki, R. Yoshimi, K. S. Takahashi, M. Kawasaki, and Y. Tokura, *Large Unidirectional Magnetoresistance in a Magnetic Topological Insulator*, *Phys. Rev. Lett.* **117**, 127202 (2016).
- [5] R. Wakatsuki, Y. Saito, S. Hoshino, Y. M. Itahashi, T. Ideue, M. Ezawa, Y. Iwasa, and N. Nagaosa, *Nonreciprocal Charge Transport in Noncentrosymmetric Superconductors*, *Sci. Adv.* **3**, e1602390 (2017).
- [6] K. Yasuda, H. Yasuda, T. Liang, R. Yoshimi, A. Tsukazaki, K. S. Takahashi, N. Nagaosa, M. Kawasaki, and Y. Tokura, *Nonreciprocal Charge Transport at Topological Insulator/Superconductor Interface*, *Nat. Commun.* **10**, 2734 (2019).
- [7] T. Guillet, C. Zucchetti, Q. Barbedienne, A. Marty, G. Isella, L. Cagnon, C. Vergnaud, H. Jaffrès, N. Reyren, J.-M. George, A. Fert, and M. Jamet, *Observation of Large Unidirectional Rashba Magnetoresistance in Ge(111)*, *Phys. Rev. Lett.* **124**, 027201 (2020).
- [8] T. Yokouchi, Y. Ikeda, T. Morimoto, and Y. Shiomi, *Giant Magnetochiral Anisotropy in Weyl Semimetal WTe₂ Induced by Diverging Berry Curvature*, *Phys. Rev. Lett.* **130**, 136301 (2023).
- [9] F. Ando, Y. Miyasaka, T. Li, J. Ishizuka, T. Arakawa, Y. Shiota, T. Moriyama, Y. Yanase, and T. Ono, *Observation of Superconducting Diode Effect*, *Nature* **584**, 373 (2020).
- [10] A. Daido, Y. Ikeda, and Y. Yanase, *Intrinsic Superconducting Diode Effect*, *Phys. Rev. Lett.* **128**, 037001 (2022).
- [11] H. Narita, J. Ishizuka, R. Kawarazaki, D. Kan, Y. Shiota, T. Moriyama, Y. Shimakawa, A. V. Ognev, A. S. Samardak, Y. Yanase and T. Ono, *Field-Free Superconducting Diode Effect in Noncentrosymmetric Superconductor/Ferromagnet Multilayers*, *Nat. Nanotechnol.* **17**, 823 (2022).
- [12] L. Bauriedl, C. Bäuml, L. Fuchs, C. Baumgartner, N. Paulik, J. M. Bauer, K.-Q. Lin, J. M. Lupton, T. Taniguchi, K. Watanabe, C. Strunk and N. Paradiso, *Supercurrent Diode Effect and Magnetochiral Anisotropy in Few-Layer NbSe₂*, *Nat. Commun.* **13**, 4266 (2022).
- [13] J.-X. Lin, P. Siriviboon, H. D. Scammell, S. Liu, D. Rhodes, K. Watanabe, T. Taniguchi, J. Hone, M. S. Scheurer, and J. I. A. Li, *Zero-Field Superconducting Diode Effect in Small-Twist-Angle Trilayer Graphene*, *Nat. Phys.* **18**, 1221 (2022).
- [14] H. Wu, Y. Wang, Y. Xu, P. K. Sivakumar, C. Pasco, U. Filippozzi, S. S. P. Parkin, Y.-J. Zeng, T. McQueen, and M. N. Ali, *The Field-Free Josephson Diode in a van Der Waals Heterostructure*, *Nature* **604**, 653 (2022).
- [15] B. Pal, A. Chakraborty, P. K. Sivakumar, M. Davydova, A. K. Gopi, A. K. Pandeya, J. A. Krieger, Y. Zhang, M. Date, S. Ju, N. Yuan, N. B. M. Schröter, L. Fu and S. S. P. Parkin, *Josephson Diode Effect from Cooper Pair Momentum in a Topological Semimetal*, *Nat. Phys.* **18**, 1228 (2022).
- [16] J. Díez-Mérida, A. Díez-Carlón, S. Y. Yang, Y. -M. Xie, X. -J. Gao, J. Senior, K. Watanabe, T. Taniguchi, X. Lu, A. P. Higginbotham, K. T. Law and D. K. Efetov, *Symmetry-Broken Josephson Junctions and*

Superconducting Diodes in Magic-Angle Twisted Bilayer Graphene, Nat. Commun. **14**, 2396 (2023).

[17] M. Trahms, L. Melischek, J. F. Steiner, B. Mahendru, I. Tamir, N. Bogdanoff, O. Peters, G. Reecht, C. B. Winkelmann, F. von Oppen and K. J. Franke, *Diode Effect in Josephson Junctions with a Single Magnetic Atom*, Nature **615**, 628 (2023).

[18] M. Masuko, M. Kawamura, R. Yoshimi, M. Hirayama, Y. Ikeda, R. Watanabe, J. J. He, D. Maryenko, A. Tsukazaki, K. S. Takahashi, M. Kawasaki, N. Nagaosa and Y. Tokura, *Nonreciprocal Charge Transport in Topological Superconductor Candidate Bi₂Te₃/PdTe₂ Heterostructure*, Npj Quantum Mater. **7**, 104 (2022).

[19] A. Sundaresh, J. I. Väyrynen, Y. Lyanda-Geller, and L. P. Rokhinson, *Diamagnetic Mechanism of Critical Current Non-Reciprocity in Multilayered Superconductors*, Nat. Commun. **14**, 1628 (2023).

[20] N. F. Q. Yuan and L. Fu, *Supercurrent Diode Effect and Finite-Momentum Superconductors*, Proc. Natl. Acad. Sci. **119**, e2119548119 (2022).

[21] S. Ilić and F. S. Bergeret, *Theory of the Supercurrent Diode Effect in Rashba Superconductors with Arbitrary Disorder*, Phys. Rev. Lett. **128**, 177001 (2022).

[22] J. J. He, Y. Tanaka, and N. Nagaosa, *A Phenomenological Theory of Superconductor Diodes*, New J. Phys. **24**, 053014 (2022).

[23] H. F. Legg, D. Loss, and J. Klinovaja, *Superconducting Diode Effect Due to Magnetochemical Anisotropy in Topological Insulators and Rashba Nanowires*, Phys. Rev. B **106**, 104501 (2022).

[24] Y. Zhang, Y. Gu, P. Li, J. Hu, and K. Jiang, *General Theory of Josephson Diodes*, Phys. Rev. X **12**, 041013 (2022).

[25] R. Kawarazaki, H. Narita, Y. Miyasaka, Y. Ikeda, R. Hisatomi, A. Daido, Y. Shiota, T. Moriyama, Y. Yanase, A. V. Ognev, A. S. Samardak, and T. Ono, *Magnetic-Field-Induced Polarity Oscillation of Superconducting Diode Effect*, Appl. Phys. Express **15**, 113001 (2022).

[26] Y. Hou et al., *Ubiquitous Superconducting Diode Effect in Superconductor Thin Films*, Phys. Rev. Lett. **131**, 027001 (2023).

[27] F.-C. Hsu, J. -Y. Luo, K. -W. Yeh, T. -K. Chen, T. -W. Huang, P. M. Wu, Y. -C. Lee, Y. -L. Huang, Y. -Y. Chu, D. -C. Yan, and M. -K. Wu, *Superconductivity in the PbO-Type Structure α -FeSe*, Proc. Natl. Acad. Sci. **105**, 14262 (2008).

[28] L.S. Farrar, M. Bristow, A.A. Haghaghirad, A. McCollam, S.J. Bending and A.I. Coldea, *Suppression of superconductivity and enhanced critical field anisotropy in thin flakes of FeSe*, npj Quantum Mater. **5**, 29 (2020).

[29] See Supplemental Material at [URL will be inserted by publisher] for reproducibility of the field-free SDE in FeSe, contact resistance analyses, simulation of thermal gradient in a FeSe flake, control experiments using FeTeSe, and fabrication process of the NbN sample.

[30] J. M. Luttinger, *Thermal Transport Coefficients of a Superconductor*, Phys. Rev. **136**, A1481 (1964).

[31] T. M. McQueen, Q. Huang, V. Ksenofontov, C. Felser, Q. Xu, H. Zandbergen, Y. S. Hor, J. Allred, A. J. Williams, D. Qu, J. Checkelsky, N. P. Ong, and R. J. Cava, *Extreme Sensitivity of Superconductivity to Stoichiometry in $Fe_{1+\delta}Se$* , Phys. Rev. B **79**, 014522 (2009).

[32] T. Watashige, Y. Tsutsumi, T. Hanaguri, Y. Kohsaka, S. Kasahara, A. Furusaki, M. Sigrist, C. Meingast, T. Wolf, H. v. Löhneysen, T. Shibauchi, and Y. Matsuda, *Evidence for Time-Reversal Symmetry Breaking of*

the Superconducting State near Twin-Boundary Interfaces in FeSe Revealed by Scanning Tunneling Spectroscopy, Phys. Rev. X **5**, 031022(2015).

[33] P. D. Lodhi, N. Kaurav, K. K. Choudhary, Y. K. Kuo, *Seebeck Coefficient Measurement and Its Narrow Band Model Interpretation in $FeTe_{0.5}Se_{0.5}$ Superconductor*, J. Supercond. Nov. Magn. **31**, 2671 (2018).

[34] Th. Siebold and P. Ziemann, *Temperature Dependence of the Thermoelectric Effect of Ion-Bombarded NbN Films: Evidence for the Suppression of Phonon Drag and for Renormalization*, Phys. Rev. B **51**, 6328 (1995).

[35] D.Y. Vodolazov and F.M. Peeters, *Superconducting rectifier based on the asymmetric surface barrier effect*. Phys. Rev. B **72**, 172508 (2005).

[36] J.R. Clem and K.K. Berggren, *Geometry-dependent critical currents in superconducting nanocircuits*. Phys. Rev. B **84**, 174510 (2011).

FIGURES and FIGURE CAPTIONS

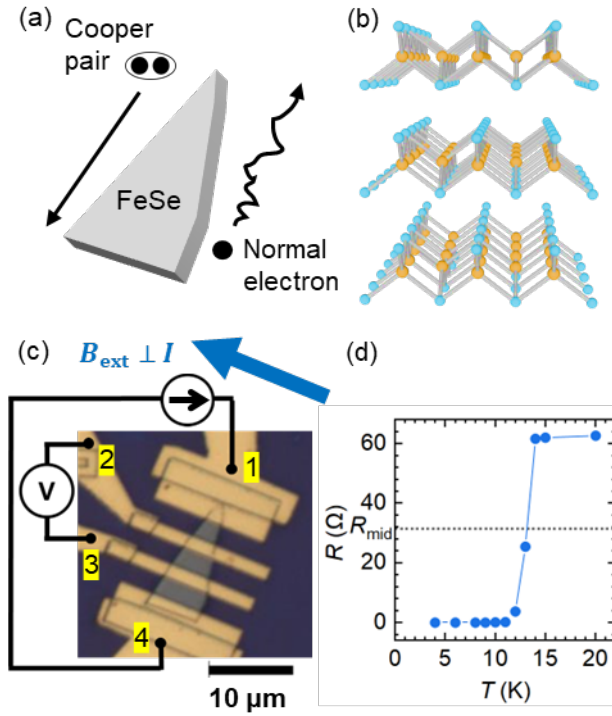


FIG. 1 (a) Schematic of the SDE in FeSe, where the Cooper pair and the normal charge current flow in opposite directions. (b) Crystal structure of FeSe. (c) Measurement setup and the fabricated device image used in our experiment. The width of electrodes 2 and 3 was $1.5 \mu\text{m}$. The absolute value of the applied current was increased from $0 \mu\text{A}$ to a maximum value in steps of $4 \mu\text{A}$. (d) Temperature dependence of the four-terminal resistance of FeSe in the device shown in (c). R_{mid} denotes the half resistance of the normal conduction resistance.

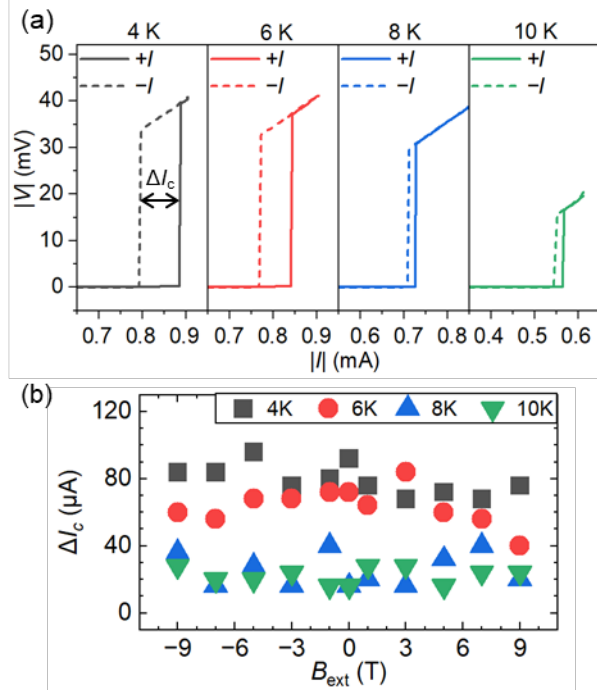


FIG. 2 (a) I - V characteristics of the device at from 4 to 10 K under positive (the solid lines) and negative (the dashed lines) electric currents. The black, red, blue, and green lines show the I - V curves at 4, 6, 8, and 10 K, respectively. An external magnetic field was not applied. (b) External magnetic field dependence of ΔI_c at temperatures ranging from 4 to 10 K. The black squares, red circles, blue up-pointing triangles, and green down-pointing triangles show the values of ΔI_c at 4, 6, 8, and 10 K, respectively.

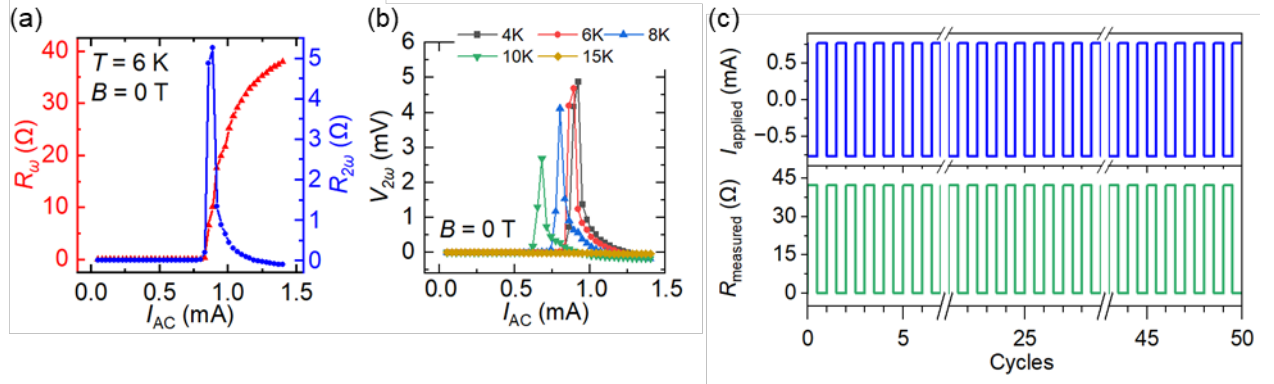


FIG. 3 (a) AC current dependence of the first (R_ω , red)- and second ($R_{2\omega}$, blue) harmonic resistances at 6 K. The frequency of the applied current was set to 17 Hz. An external magnetic field was not applied. (b) AC current dependence of the second-harmonic voltages at various temperatures. The black, red, blue, green, and yellow lines show the results at 4, 6, 8, 10, and 15 K, respectively. (c) Half-wave rectification results between the superconducting and normal conducting states demonstrated at 6 K without an external magnetic field. The upper panel shows the cycles of the applied current I_{applied} between electrodes 1 and 4. The amplitude of I_{applied} is 0.77 mA (between I_{c+} and $|I_{c-}|$). The lower panel shows the measured resistance R_{measured} between electrodes 2 and 3 when the current flows.

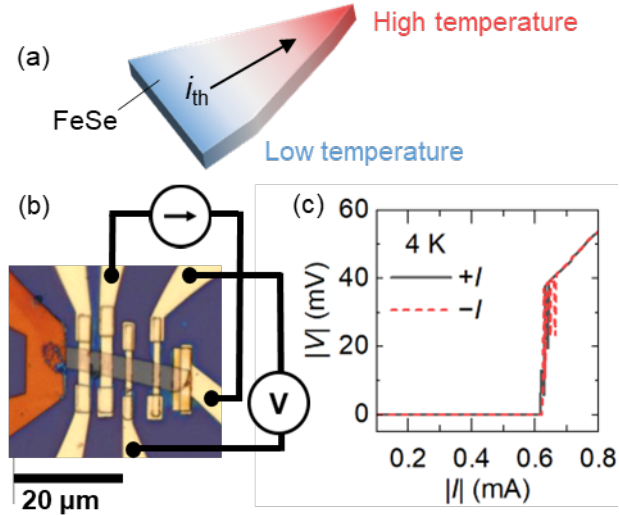


FIG. 4 (a) Schematic of a thermal gradient in FeSe, resulting in an additional current flow. i_{th} denotes the thermoelectric current generated by the thermal gradient. (b) Measurement setup and fabricated device equipped with a symmetric FeSe superconducting channel. An external magnetic field is not applied. (c) I - V characteristics of the FeSe device shown in (b) at 4 K under positive (black solid lines) and negative (red dashed lines) electric current injection. The absolute value of the applied current was increased from 0 mA in 0.004 mA steps. The field-free SDE is not observed.

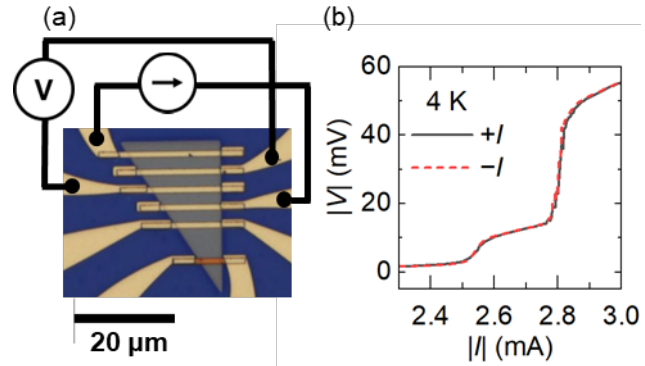


FIG. 5 (a) Measurement setup and the fabricated device for the control experiment using NbN. The thickness of the NbN is 103 nm. An external magnetic field is not applied. (b) I - V characteristics of the NbN device at 4 K under positive (black solid line) and negative (red dashed line) electric current injection. The absolute value of the applied current was increased from 0 mA in 0.004 mA steps. The field-free SDE is not observed.